High Temperatures – High Pressures, 2002, volume 34, pages 515 – 521

DOI:10.1068/htjr061

Improvement of the mathematical modeling of flash measurements

Jürgen Blumm, Johannes Opfermann
NETZSCH-Gerätebau GmbH, Wittelsbacherstraße 42, D-95100 Selb, Bavaria, Germany;
fax: 49-9287-881-144; email: j.blumm@ngb.netzsch.com
Presented at the 16th European Conference on Thermophysical Properties, Imperial College, London, England, 1 – 4 September 2002

Abstract. The laser flash technique allows measurement of the thermal diffusivity of solids and liquids up to very high temperatures. Various mathematical models have been developed over the past few decades to analyse the experimental data and to remove the influence of the pulse length of the laser and heat loss effects. The most sophisticated model was established by Cape and Lehman (1963 *J. Appl. Phys.* **34** 1909 – 1913) which considers finite pulse effects as well as facial and radial heat losses. For simplification, various assumptions were made in this work to achieve an analytical solution. Improvements of the assumptions were made by other authors such as Josell et al (1995 *J. Appl. Phys.* **78** 6867 – 6868). Further improvements are proposed here. For accurate pulse-length correction, the original laser pulse is monitored by the hardware and used in the analysis. Furthermore, some improved approximations were integrated into the model. Finally, higher-order solutions of the mathematical description are considered in the analysis. The improved mathematical model is integrated in the nonlinear regression routine, allowing fitting of experimental data to yield thermal diffusivity values with high accuracy.

1 Introduction

Over the past few decades the flash method (Parker et al 1961) has become the most widely used technique for the measurement of the thermal diffusivity of various kinds of solids, powders, and liquids. In this technique, the front face of a small, usually disk-shaped, plane-parallel sample is heated by a short energy (laser) pulse. The temperature rise at the rear surface is measured versus time with an infrared detector. Easy sample preparation, small required sample dimensions, fast measurement times, and high accuracy are only a few of the advantages of this non-contact and non-destructive measurement technique. By placing the sample in a tubular furnace, temperature-dependent measurements can be easily realised. Since the introduction of the method by Parker et al (1961) new models for processing the raw data have been developed. Mathematical algorithms have been created to correct for heat loss (Cowan 1963) and finite pulse effects (Azumi and Takahaski 1981). One of the most sophisticated mathematical models was developed by Cape and Lehman (1963) in which both radial and facial heat losses as well as finite pulse effects were considered. It is based on the solution of the transient heat conduction equation in cylindrical coordinates with radiative heat losses from all surfaces used as boundary conditions. To solve this equation several simplifications and approximations were employed. In the last few years several improvements were published for these approximations, for example by Josell et al (1995).

2 The improved mathematical model

In this work we present an improved mathematical model for the treatment of laser flash data. It is based on the theoretical model developed by Cape and Lehman (1963) for a cylindrical sample with account taken of both facial and radial heat losses.

The heat losses from the front and rear surfaces, as well as from the surrounding area, are considered as radiative heat losses as already described in the solution of Cape and Lehman (1963):

$$T(r,\,t) = T_\infty \sum_{m=0}^{\infty} C_m X_m \sum_{i=0}^{\infty} D_i(r,\,Y_r) \int_0^t \mathrm{d}\tau W(\tau) \exp[\omega_{im}(t-\tau)/t_c] \ . \tag{1}$$

Here, $T(r,\,t)$ is the temperature rise at the rear surface of the sample as a function of time t and radial location r; T_∞ is the signal rise under isothermal conditions at infinite times; C_m and X_m are parameters accounting for the facial heat loss and will be discussed later; $W(\tau)$ is the pulse shape of the laser employed for the tests; τ is the pulse length of the laser. Analysis of $W(\tau)$ will be discussed later. The quantities Y_r will be called radial Biot numbers and describe the amount of radial radiative heat loss:

$$Y_r = 4\sigma\varepsilon_r T_0^3 \lambda^{-1} r_0 \ . \tag{2}$$

Here, σ is the Stefan–Boltzmann constant and ε is the total emissivity of the sample; T_0 is the sample temperature, and λ its thermal conductivity; r_0 is the radius of the sample. Other parameters such as ω_{im} and t_c will be explained afterwards. The coefficients $D_i(r,\,Y_r)$ define the amount of radial heat loss over the outer cylinder surfaces. For $Y_r = 1$, the zero-order solution $D_0(r,\,Y_r)$ gives approximately 96% of all contributions of this series (Cape and Lehman 1963). The solution used in this work makes additional use of the contributions of $D_1(r,\,Y_r)$ and $D_2(r,\,Y_r)$ to reduce the influence of high heat losses at high temperatures. Therefore, more than 99% of the contributions of $D_i(r,\,Y_r)$ on the final result are considered.

$$D_i(r,\,Y_r) = \frac{2\,Y_r}{Y_r^2 + z_i^2(Y_r)} \frac{J_0\left(z_i \dfrac{r}{r_0}\right)}{J_0(z_i)} \ . \tag{3}$$

The J_x are the Bessel functions; r is the radial location between the centre of the sample and the point where the temperature rise should be determined. The z_i will be discussed later. Equation (3) can be simplified if only the temperature rise in the centre of the sample is considered. In this case equation (3) reduces to:

$$D_i(Y_r) = \frac{2\,Y_r}{Y_r^2 + z_i^2(Y_r)} \frac{1}{J_0(z_i)} \ . \tag{4}$$

The z_i in equations (3) and (4) are defined as the positive roots of equation (5):

$$Y_r J_0(z_i) = z_i J_1(z_i) \ . \tag{5}$$

For high accuracy, it was necessary to obtain z_i by numerical procedures which were time-consuming and therefore not useful for practical applications such as fast nonlinear regression routines. In this work another approach was used which was already mentioned by Cape and Lehman (1963). The exact dependence between Y_r and z_i^2 was calculated for different Y_r and z_i. z_i^2 was used here as this is the parameter required in equation (4) for the determination of $D_i(Y_r)$. The resulting points were fitted with polynomial functions. By using these functions, determination of $z_i^2(Y_r)$ is now much easier and faster. To achieve a high level of accuracy, higher-order polynomials were used for the approximations. The functions for z_0^2, z_1^2, and z_2^2 were found to be:

$$z_0^2 = Y_r \begin{pmatrix} 2 - 0.4999763\,Y_r + 8.3226814 \times 10^{-2}\,Y_r^2 - 4.9728037 \times 10^{-3}\,Y_r^3 \\ - 1.860453 \times 10^{-3}\,Y_r^4 + 6.860453 \times 10^{-4}\,Y_r^5 - 1.1883159 \times 10^{-4}\,Y_r^6 \\ + 1.2014985 \times 10^{-5}\,Y_r^7 - 6.6548853 \times 10^{-7}\,Y_r^8 + 1.5096279 \times 10^{-8}\,Y_r^9 \end{pmatrix}, \tag{6}$$

and

$$z_1^2 = 14.6819727 + 1.9997132\,Y_r + 1.5060371 \times 10^{-3}\,Y_r^2 - 4.8256703 \times 10^{-2}\,Y_r^3 - 7.2545466 \times 10^{-3}\,Y_r^4 + 9.17296 \times 10^{-5}\,Y_r^5 - 1.6307912 \times 10^{-4}\,Y_r^6 + 2.0403799 \times 10^{-5}\,Y_r^7 - 8.6861677 \times 10^{-7}\,Y_r^8 \ , \tag{7}$$

$$z_2^2 = 49.2184560 + 2.0000018\,Y_r - 1.3546218 \times 10^{-2}\,Y_r^3 + 4.0869796 \times 10^{-4}\,Y_r^4 + 1.6084755 \times 10^{-4}\,Y_r^5 - 1.9378177 \times 10^{-5}\,Y_r^6 + 6.0429595 \times 10^{-7}\,Y_r^7 \ . \tag{8}$$

The difference between the real z_i^2 and the z_i^2 determined by the above equations is in all cases better than 2.5×10^{-7} (least squares). This good correlation between the exact z_i^2 and the ones determined by equations (6) to (8) can be seen in figure 1. No differences are visible between the exact values and the calculated ones.

It must be pointed out that, when the above approximations are used, one problem can arise. For no radial heat loss, z_0 and Y_r go to 0. Therefore, $D_0(Y_r)$ will no longer be defined (0 divided by 0). To overcome this problem, a boundary analysis was carried out, resulting in:

$$\lim_{Y_r \to 0} [D_0(Y_r)] \to \frac{1}{1 + 0.25\,Y_r} \ . \tag{9}$$

Another factor required for solving equation (1) are the products $C_m X_m$. These parameters are defined by equation (10) (Cape and Lehman 1963).

$$C_m X_m = (-1)^m \frac{2a}{d} \frac{X_m^2}{X_m^2 + 2\,Y_x + Y_x^2} \ . \tag{10}$$

Here a is the thermal diffusivity of the sample; d is the thickness of the sample; Y_x can be described as the facial Biot number. Y_x is defined in a similar way to equation (2), by exchanging r_0 for the sample thickness d. The X_m are defined as the positive roots of equation (11):

$$(X_m^2 - Y_x^2)\tan(X_m) - X_m Y_x = 0 \ . \tag{11}$$

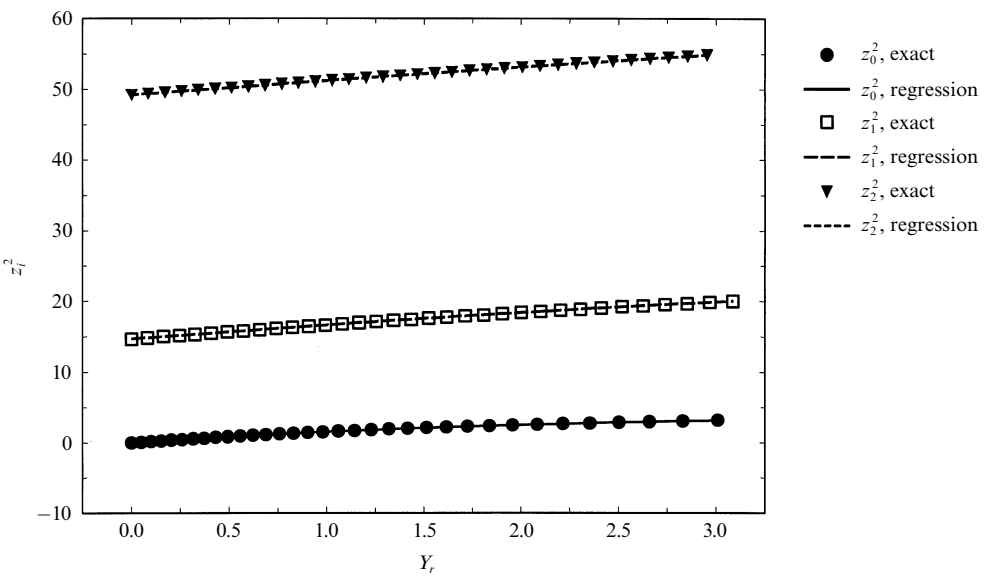

Figure 1. Comparison between the exact values of z_i^2 and the z_i^2 determined with equations (6) to (8).

Again, the determination of the exact dependence between Y_x and X_m requires numerical approaches. Therefore, Cape and Lehman (1963) already offered the first approach for obtaining $X_m(Y_x)$ from approximated polynomials. These polynomials were then improved by Josell et al (1995). Here, we improved further the accuracy of the X_m. We used the following equations:

$$X_0 = \left[(2Y_x)\left(1 - \frac{Y_x}{6} + \frac{Y_x^2}{45} - \frac{2Y_x^3}{945} + \frac{Y_x^4}{14175} + \frac{2Y_x^5}{93555} - \frac{1082Y_x^6}{212837625}\right)\right]^{1/2} , \tag{12}$$

$$\begin{aligned} X_m = {} & \frac{m}{\pi} + 2\frac{Y_x}{\pi m} - \frac{4Y_x^2}{(\pi m)^3} + \frac{2}{3}\left[\frac{24-(\pi m)^2}{(\pi m)^5}\right]Y_x^3 - \frac{16}{3}\left[\frac{15-(\pi m)^2}{(\pi m)^7}\right]Y_x^4 \\ & + \frac{2}{5}\left[\frac{1120-100(\pi m)^2+(\pi m)^4}{(\pi m)^9}\right]Y_x^5 - \frac{4}{15}\left[\frac{10080-1120(\pi m)^2+23(\pi m)^4}{(\pi m)^{11}}\right]Y_x^6 \\ & + \frac{2}{315}\left[\frac{2661120-352800(\pi m)^2+10976(\pi m)^4-45(\pi m)^6}{(\pi m)^{13}}\right]Y_x^7 \\ & - \frac{704}{105}\left[\frac{16380-2520(\pi m)^2+105(\pi m)^4-(\pi m)^6}{(\pi m)^{15}}\right]Y_x^8 \\ & + \frac{2}{63}\left[\frac{2306040-4036032(\pi m)^2+210672(\pi m)^4-3272(\pi m)^6+7(\pi m)^8}{(\pi m)^{17}}\right]Y_x^9 \\ & - \frac{4}{945}\left[\frac{1176215040-230630400(\pi m)^2+14462448(\pi m)^4-315920(\pi m)^6+1689(\pi m)^8}{(\pi m)^{19}}\right] \\ & \times Y_x^{10} . \end{aligned} \tag{13}$$

Using the new functions, an improved correlation between the exact X_m and the ones used for the calculations could be found especially for high heat losses. Table 1 provides a comparison of exact X_m values with those determined by others and the ones calculated in this work. It can be clearly seen that the new functions provide accurate values of the required X_m.

Table 1. Comparison of the quality of the approximations for X_m in equation (1) by different authors.

Biot number, Y_x ($m = 1$)	Exact solution	Cape and Lehman (1963)	Josell et al (1995)	This work
0.05	3.1731049	3.1724	3.173105	3.1731049
0.50	3.4310143	3.3539	3.430933	3.4310141
1.00	3.6731944	3.3607	3.670930	3.6731945
1.50	3.8794820	3.2316	3.864288	3.8794819

ω_{im} in equation (1) is defined in the following way:

$$\omega_{im} = -\left(\frac{d}{\pi}\right)^2\left(\frac{X_m^2}{d^2} + \frac{z_i^2}{r_0^2}\right) ; \tag{14}$$

t_c, which also appears in equation (1), is the characteristic time required for a heat pulse to propagate through a sample of thickness d:

$$t_c = \left(\frac{d}{\pi}\right)^2\frac{1}{a} . \tag{15}$$

As can be seen from figure 1, z_i^2 sharply increases with increasing i; ω_{im} increases in the same way with i. Because of this, higher-order solutions of z_i^2 (z_3^2, z_4^2, ...) yield only negligible contributions to ω_{im} in equation (1) and are not considered here.

The last quantity not defined in equation (1) is the pulse shape $W(\tau)$ of the laser employed for the tests. Generally, the pulse shape and length are approximated by simplified square or triangle functions. Of course, these approximations are rough and do not take into account the real pulse shape of the laser. Furthermore, any changes of the laser pulse shape with time or with the laser settings are difficult to consider. The NETZSCH model LFA 427 used in this work has an integrated laser pulse diode, allowing measurement of the laser pulse shape for each individual measurement. This allowed us to check the relationship between laser settings and pulse shape. A mathematical model was developed allowing accurate pulse description, and therefore pulse-length correction, for the laser system employed here. A combination of different exponential functions with different time constants was employed:

$$\begin{aligned} W(\iota) &= A[1 - \exp(-\iota/l_1)\exp(-\iota/l_2)], \quad \iota \leqslant t_e \\ W(\tau) &= A\{1 - \exp(-t_e/l_1)\exp(-t_e/l_2)\exp(-[\tau - t_e]/l_3)\}, \quad \tau > t_e \ . \end{aligned} \tag{16}$$

A is the signal height of the output of the laser diode. The different l_i describe the different time constants occurring in different stages of the laser power output (start, intermediate, end). The characteristic time t_e is the time when the power input into the flash lamps is switched off and the power output exponentially goes down to 0. By optimising the different parameters of equation (16) by a nonlinear regression routine on the measured pulse shape, the mathematical model can be adjusted to reproduce the real pulse shape of the laser shot employed for the tests.

Figure 2 provides a comparison between a measured pulse shape of the LFA 427 (Bräuer et al 1992) and calculations made by the nonlinear regression process. The laser of the LFA was set to a pulse length of 0.8 ms. Data acquisition was started when the laser received the command to fire. After approximately 0.1 ms, the power output of the laser starts. The onset of this power output is determined and used as the zero point for the time axis of the detector signal. The result of the nonlinear regression

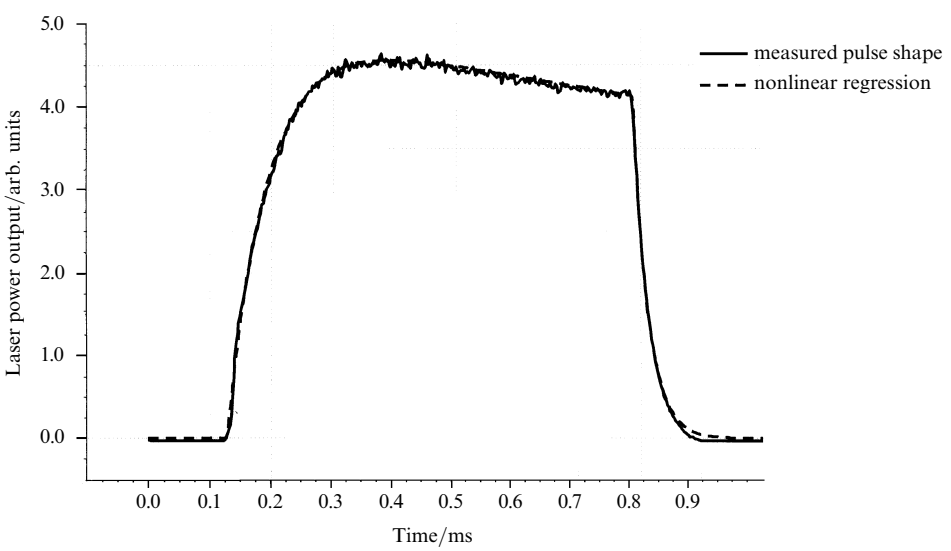

Figure 2. Comparison between the measured pulse shape and the result of a nonlinear regression process based on equation (16). The nominal pulse width was 0.8 ms.

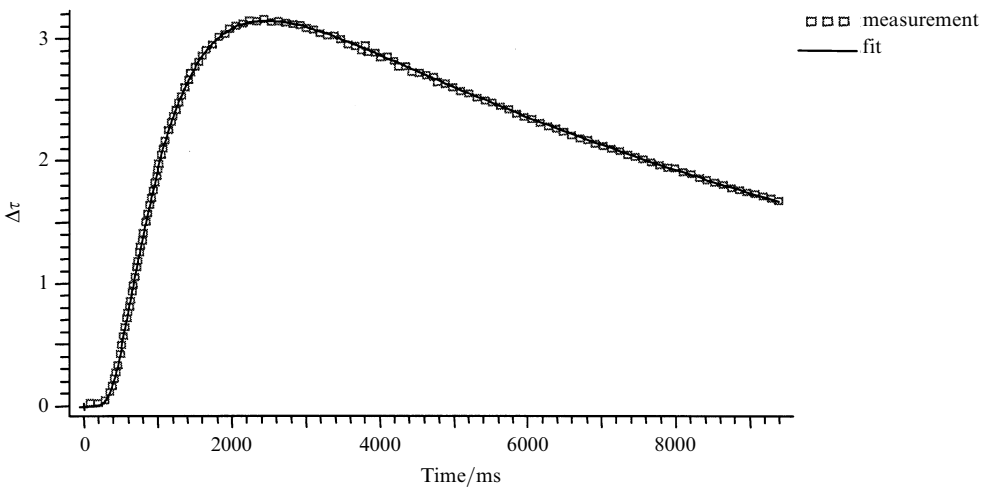

Figure 3. Application of the nonlinear regression (fitting) process (line) to test result on Pyroceram 9606 (squares) making use of the new mathematical model.

routine on the measured pulse shape (figure 2) is used as $W(\tau)$ in equation (1). Therefore, the optimum pulse-length correction is guaranteed.

Application of nonlinear regression to a measurement made on Pyroceram 9606 at 900 °C is shown in figure 3. The nonlinear regression process was based on a modified Levenberg – Marquardt (Opfermann 1985) algorithm. It can be clearly seen that the new model provides an accurate description of the resulting temperature rise at the rear face as well as the heat loss effects. As a result of the fitting process, the thermal diffusivity and the radial/facial heat loss factors can be derived with maximum possible accuracy.

To check the accuracy of the new mathematical modeling, a theoretical curve was calculated with a finite-element simulation software (Ansys™). Several calculations were done for samples with different emissivities and at different temperatures. The resulting curves were analysed with a nonlinear regression routine on the basis of equation (1). With the new model, the theoretical values for the thermal diffusivity were found to be within the accuracy of the FEM simulations.

Figure 4 shows the calculated curve (squares) and the nonlinear regression applied to the theoretical curve. A disk-shaped sample with a thickness of 4 mm, diameter of 12.7 mm, emissivity of 93% on all surfaces, density of 1.655 g cm^{-3}, specific heat of 2.136 J g^{-1} K^{-1}, and thermal diffusivity of 10.55 mm^2 s^{-1} was employed for the simulations. Such values would be typical for graphite samples. The simulation was carried out for a temperature of 2000 °C. The laser pulse was approximated by a constant-power input with a duration of 0.5 ms. It can be clearly seen that there is no difference between the two curves. The resulting thermal diffusivity was within 1.5% of the original value used for the FEM modeling. It must be pointed out that the difference between the simulation and the nonlinear regression routine is mainly due to the limited time and temperature accuracy of the simulated curve.

3 Conclusion

An existing mathematical model for the analysis of the detector signals in laser flash measurements was optimised. Improved accuracy in the approximations of the individual parameters leads to increased accuracy of the results at high temperatures. Analysis of the real pulse shape employed for the individual test and integration of this in the pulse-length correction results in a further improvement of the accuracy of the results at short measurement times.

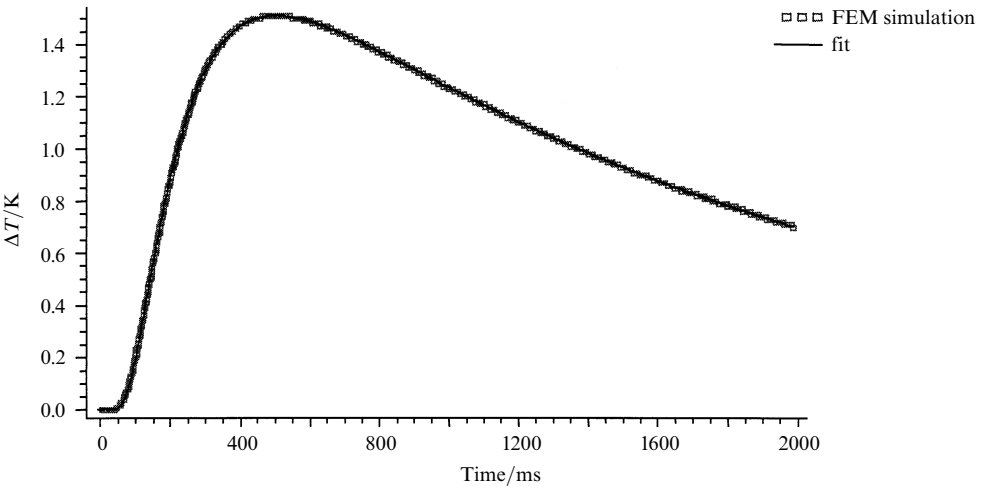

Figure 4. Nonlinear regression (fitting) process (line) together with a theoretical curve calculated by FEM simulation.

References

Azumi T, Takahaski Y, 1981 *Rev. Sci. Instrum.* **52** 1411 – 1413
Bräuer G, Dusza L, Schulz B, 1992 *Interceram* **42** 489 – 492
Cape J A, Lehman G W, 1963 *J. Appl. Phys.* **34** 1909 – 1913
Cowan R D, 1963 *J. Appl. Phys.* **34** 926 – 929
Josell D, Warren J, Cezairliyan A, 1995 *J. Appl. Phys.* **78** 6867 – 6868
Opfermann J R, 1985 *Rechentechnik/Datenverarbeitung* **22**(3) 26 – 27
Parker W J, Jenkins R J, Butler C P, Abbott G L, 1961 *J. Appl. Phys.* **32** 1679 – 1684